energies

MDPI

Article

Experimental Investigation of Wall Confluent Jets on Transparent Large-Space Building Envelopes: Part 2—Application in Cooling Greenhouses

Gasper Choonya [1,*], Alan Kabanshi [1] and Bahram Moshfegh [1,2]

[1] Department of Building Engineering, Energy Systems and Sustainability Science, University of Gävle, 801 76 Gävle, Sweden; alan.kabanshi@hig.se (A.K.); bahram.moshfegh@hig.se or bahram.moshfegh@liu.se (B.M.)
[2] Department of Management and Engineering, Division of Energy Systems, Linköping University, 581 83 Linköping, Sweden
* Correspondence: gasper.choonya@hig.se

Abstract

This study experimentally evaluated the performance of a wall confluent jet (WCJ) cooling system in a greenhouse under real summer and autumn weather conditions. It examined the effects of indoor air temperature setpoint (T_{spt}), number of nozzle rows (n) on the WCJ diffuser, and external wall shading on WCJ's cooling performance. Thermocouples and constant-current anemometers measured air and surface temperatures and air velocity, while pyranometers measured solar radiation. The WCJ system dynamically regulated inlet air temperature between 14 °C and 25 °C to counter solar and conductive heat gains, maintaining indoor air temperature within ±1.5 °C of the setpoint. Increasing T_{spt} by 4 °C reduced inlet cooling demand by 25% but increased indoor air temperature by 20–25% and raised ceiling, wall, and floor surface temperatures by 17%, 20%, and 16%, respectively. Increasing n reduced surface temperatures by up to 8% and indoor air temperature by 6%. External wall shading reduced solar heat gain, lowering interior surface temperatures by 10–30%, peak and mean indoor air temperatures by up to 35% and 15%, and net power peaks by 40%. Autumn conditions reduced cooling loads by 50% relative to summer. Overall, WCJ cooling demonstrates strong potential as an alternative or complementary system for greenhouse thermal regulation without increasing primary energy demand.

Keywords: wall confluent jets; experimental field study; greenhouse cooling; indoor environment; greenhouse envelope shading

Check for updates

Academic Editor: Boris Igor Palella

Received: 22 December 2025
Revised: 3 February 2026
Accepted: 5 February 2026
Published: 7 February 2026
Corrected: 18 May 2026

Copyright: © 2026 by the authors. Licensee MDPI, Basel, Switzerland. This article is an open access article distributed under the terms and conditions of the Creative Commons Attribution (CC BY) license.

1. Introduction

Transparent external envelopes, widely used in large-scale space-enclosure buildings such as airports [1], sports arenas, shopping malls, and greenhouses [2–4], enhance aesthetics and natural light, supporting human social interactions. In contrast, they are integrated in greenhouses to create controlled environments for crops, rather than for human occupancy [5,6]. Greenhouse fully glazed envelopes maximize daylight but also transmit large fractions of solar radiation, leading to elevated indoor temperatures and a strong dependence on external climatic conditions. With low thermal buffering, transparent envelopes transmit shortwave solar radiation and re-radiate it as longwave infrared radiation, producing a greenhouse effect that often results in higher indoor temperatures [7–9].

Creating an indoor thermal environment free of excessive heat, which can decrease crop stress, reduce water demand, and increase productivity, is challenging [10]. Green-

 https://doi.org/10.3390/en19040875

house cooling demand often exceeds heating demand, particularly in regions with intense solar radiation and during summer, posing significant challenges for crop health and productivity [11]. Conventional greenhouse cooling methods include natural ventilation, shading, and evaporative cooling systems [12,13]. While passive strategies (e.g., shading, coating, natural ventilation) are low-cost, their cooling performance declines in hot climates, and some may reduce light transmission. Active systems such as evaporative cooling systems provide reliable control but are energy- and cost-intensive. More advanced techniques, such as earth-to-air exchangers or aquifer storage, are currently limited by infrastructure requirements and site-specific constraints [12].

The wall confluent jet (WCJ) integrated cooling system offers a promising alternative for greenhouse environments. WCJ systems evolve from confluent jets (CJs), in which multiple parallel air streams from adjacent nozzles merge into a single coherent jet that attaches to nearby surfaces via the Coandă effect [14,15] and follows the surface contour. As the WCJ propagates, the no-slip boundary condition enforces zero velocity at the surface while velocity increases away from it, forming a boundary layer. Within this layer, shear forces between adjacent fluid layers arise, promoting convective heat transfer through turbulent mixing. At the air–surface interface, conductive heat transfer dominates, facilitating thermal exchange between the jet and the surface. Meanwhile, at the outer jet layers, the entrainment of ambient room air predominates, leading to heat exchange between the WCJ and the surrounding room air [15,16].

Earlier studies have demonstrated that CJ and WCJ generate high-momentum flows that enhance air distribution, conserve momentum, and reduce thermal stratification, with WCJ outperforming traditional mixing and displacement systems by providing more uniform temperatures, deeper jet penetration, improved contaminant removal, and higher energy efficiency [17–19]. Integrating CJ diffusers with impinging jets further strengthens WCJ penetration and thermal control in large enclosures [20]. Turbulent-flow studies of unconfined CJs identify a confluent core zone characterized by uniform streamwise velocity and reduced velocity decay [21]. Near-field investigations reveal that nozzle positioning (central, side, or corner) significantly influences entrainment, momentum transfer, velocity decay, and lateral dispersion [22]. Recent research has confirmed the effectiveness of WCJ for greenhouse heating using low-grade waste heat [23]. However, evidence on their cooling performance in greenhouse premises remains scarce.

This field study evaluated the performance of a wall confluent jets (WCJ) air-based cooling system in a full-scale greenhouse under transient Nordic summer–autumn conditions. Specifically, we quantified how (i) the number of nozzle rows on the WCJ diffuser (n), (ii) the greenhouse air-temperature setpoint (T_{spt}), and (iii) external-wall shading influence the system's ability to control the plant-occupied zone microclimate (temperature and air movement). The study addresses the application of air-based cooling systems based on wall-confluent jets in large-space enclosures, with a field study on greenhouses.

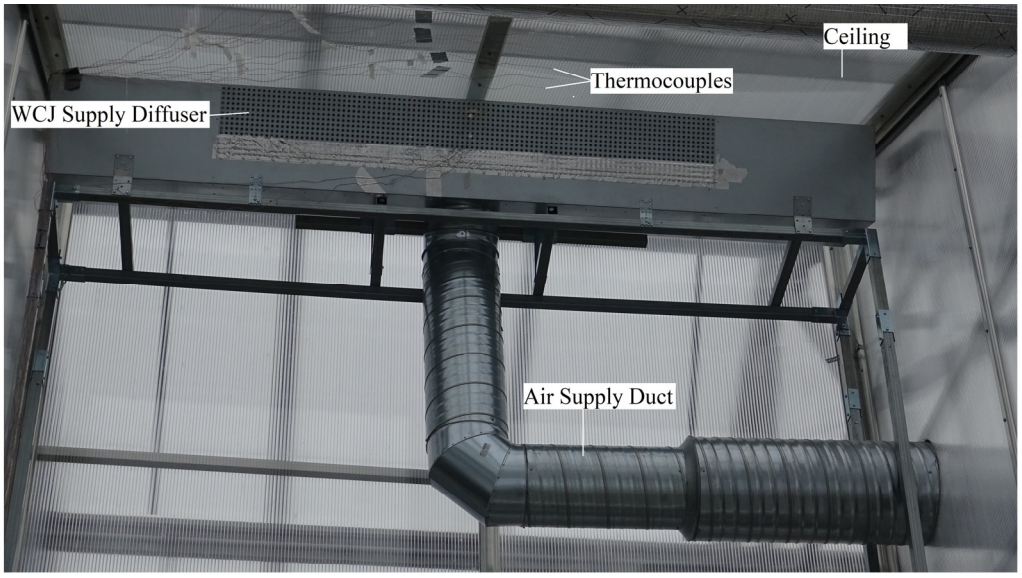
2. Materials and Methods

2.1. Research Facility

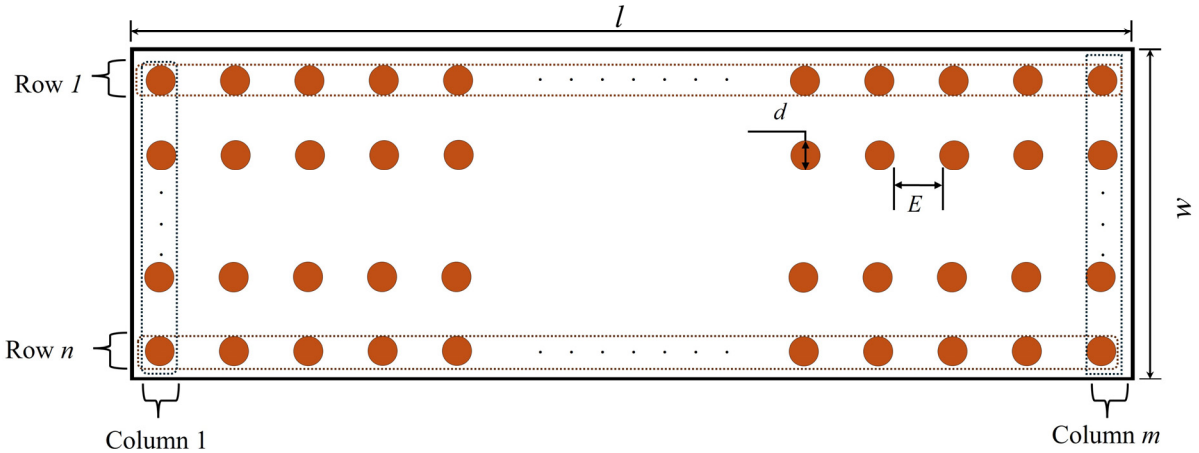
In this study, experiments were conducted in an empty, typical north–south-oriented gable-type greenhouse located in Hofors (60.5460° N, 16.2841° E) in central Sweden. The test room was a partition within the main greenhouse, with three walls enclosed by the greenhouse and the roof, and the external wall exposed to the outdoor environment. The partitioned test room measured 6.6 m in length, 2.8 m in width, with a gable height of 6.6 m and an eave height of 4 m. It featured a 7.1 m long roof sloping at 26° from the eave, forming the external wall. The three sidewalls were shaded with 95% reflective aluminum film to minimize thermal interference from the main greenhouse, while the external wall and roof

remained exposed to outdoor conditions. The external wall was alternately shaded and unshaded using the same reflective aluminum films, as part of the experimental boundary conditions. The greenhouse envelope consisted of 0.016 m thick transparent honeycomb polycarbonate, a material with a typical U-value of 1.95 W/m^2·K, suitable for greenhouse applications. The floor comprised a 0.1 m thick concrete layer.

The WCJ diffuser was mounted 0.03 m below the ceiling on the gable wall at a height of 6.57 m. The diffuser plate (1.62 m × 0.30 m) contained an array of nozzles with a diameter d = 0.0058 m and a spacing between nozzles E = 1.82d. The WCJ diffuser distributed conditioned air supplied through a 0.25 m diameter duct. The air exited the test room through a 0.4 m diameter exhaust duct installed at 4.0 m above the floor on the same wall as the WCJ diffuser. Figure 1a shows a photo of the installed WCJ diffuser in the test room. Figure 1b shows the details of the representative WCJ diffuser.



(a)



(b)

Figure 1. (**a**) Picture of the installed WCJ diffuser and supply air duct; (**b**) WCJ diffuser nozzle plate with representative nozzles. Note: d is the interior diameter of the nozzle, E is the spacing between adjacent nozzles, w is the width of the nozzle plate, l is the length of the nozzle plate, n is the number of nozzle rows, and m is the number of nozzle columns.

The diffuser used modular nozzle plates with adjustable dimensions (w and l) that allowed control of the number of nozzle rows (n) and could be linked together to achieve the overall length needed for the specified number of nozzle columns (m).

2.2. Air Handling Unit

A fan circulated air through a closed loop comprising the test room and an air-handling unit (AHU) with a cooling capacity of 5 kW. Two modulating dampers controlled the distribution of inlet airflow rate into the test room, while return air was filtered and recirculated through the system. A dedicated chilled water circuit, featuring a chiller, a 0.15 m^3 buffer tank, and a centrifugal pump, was employed to supply cold water to the heat exchanger unit, thereby enhancing the AHU's cooling performance. Chilled water circulated between the buffer tank and the cooling unit. Valves and a cooling coil controlled the flow and thermal conditions, which were monitored using pressure sensors and PT100 RTDs at the heat exchanger inlet and outlet, as well as along the ductwork. A room air temperature setpoint (T_{spt}) sensor (accuracy: $\pm$[0.3 °C + 0.005 × |t|], range: 0–150 °C), provided feedback for cooling coil modulation. The cooling coil dynamically adjusted the inlet air temperature (T_{in}) to maintain the indoor air setpoint (T_{spt}), compensating for heat gains from the external environment.

2.3. Experimental Setup

Preliminary experiments evaluating the cooling capacity of the WCJ-integrated AHU were conducted in April and May 2024 to validate system functionality and establish baseline performance. These results indicated that the AHU's cooling element had a limited cooling effect at low airflow rates. Comprehensive field measurements assessing WCJ cooling performance were conducted during summer (June–August 2024) and extended into autumn (September–October 2024).

The study included 27 field experiments, referred to as runs, each defined by a unique combination of inlet airflow rate ($\dot{V}$), number of nozzle rows (n), and room air temperature setpoint (T_{spt}). The AHU's installed cooling capacity limited the inlet airflow rate, which was held constant at $\dot{V}$ = 0.4 m^3/s for all experiments. Three nozzle configurations (n = 8, 10, and 12 rows), a fixed number of columns (m = 98), and three temperature setpoints (T_{spt} = 22 °C, 24 °C, and 26 °C) were deployed to yield nine foundational runs. The experimenters varied the seasonal climatic conditions and the status of external wall shading in the nine foundational runs, producing a total of 27 runs. The 27 field experiments are categorized as follows:

I. Summer experiments without shading on the outer surface of the external wall.
II. Summer experiments with shading on the outer surface of the external wall.
III. Autumn experiments without shading on the outer surface of the external wall.

Table 1 summarizes the 27 runs by organizing them according to weather conditions, the shading status of the test room's external wall, the number of nozzle rows, and the indoor air temperature setpoint.

Table 1. 27 field experiments (runs) conducted in the study.

Run	Airflow Rate $\dot{V}$ [m^3/s)]	Room Air Temperature Setpoint (T_{spt}) [°C]	Number of Nozzle Rows (n) [-]
Summer_Unshaded External Wall			
1	0.4	22	8
2	0.4	24	10
3	0.4	26	12
4	0.4	22	12

Table 1. *Cont.*

Run	Airflow Rate $\dot{V}$ [m^3/s)]	Room Air Temperature Setpoint (T_{spt}) [°C]	Number of Nozzle Rows (n) [-]
5	0.4	24	8
6	0.4	26	10
7	0.4	22	10
8	0.4	24	12
9	0.4	26	8
Summer_Shaded External Wall			
10	0.4	22	8
11	0.4	24	10
12	0.4	26	12
13	0.4	22	12
14	0.4	24	8
15	0.4	26	10
16	0.4	22	10
17	0.4	24	12
18	0.4	26	8
Autumn_Unshaded External Wall			
19	0.4	22	8
20	0.4	24	10
21	0.4	26	12
22	0.4	22	12
23	0.4	24	8
24	0.4	26	10
25	0.4	22	10
26	0.4	24	12
27	0.4	26	8

The runs enable systematic analysis of WCJ cooling performance across varying heat-gain scenarios. The T_{spt} range of 22 °C to 26 °C was selected because it falls within the recommended indoor greenhouse air temperature range for summer [24,25].

2.4. Air Velocity and Temperature Measurement

Thermocouples measured surface and room air temperatures, while constant-current anemometers (CCAs) measured the velocity and temperature of the WCJ across various zones of the test room. Each run began with a 12 h stabilization period, followed by data recording every 60 s for a 24 h measurement phase.

2.4.1. Measurements with Constant Current Anemometers (CCAs)

The CCAs measured the velocity and temperature of the air in the boundary layers formed by the WCJ along the surfaces in three zones: Zone I (ceiling), Zone II (inner surface of the external wall), and Zone III (floor). CCAs were selected for their high sensitivity, rapid response time, and robust performance, and their broader use in meteorological, aerodynamic, and HVAC research applications [26,27]. The WCJ from the diffuser first flowed parallel to the ceiling, merged at a certain downstream point, adhered to the ceiling surface via the Coandă effect, and remained attached until it reached the ceiling–external wall adjoining corner. Then, the WCJ deflected downwards, re-attached, and descended along the inner surface of the external wall until it reached the external wall–floor adjacent corner. The WCJ impinged on the floor, spread across it, and eventually exited the test room through the exhaust duct.

Thirty-two custom-fabricated CCAs were deployed at different positions across the three zones. Each probe integrated a 0.3 mm Honeywell 111-202CAK-H02 velocity sensor accurate to ±5%, with a time constant of 0.5 s at 0.5 m/s and 0.1 s at 20 m/s and a B43-K-5

thermometric sensor, digitally calibrated for temperatures up to 40 °C with ±0.05 °C accuracy. Digi-Key Electronics in Thief River Falls, Minnesota, USA, manufactures this type of velocity sensor. Thermometrics Corporation in Northridge, California, USA, manufactured this type of temperature sensor. The researchers calibrated all CCAs in an open-circuit wind tunnel under controlled conditions to ensure measurement accuracy. They connected the sensors to a 32-channel anemometer data logger, which was controlled via LabVIEW 2017. A previous study [23] provides further details on sensor operation. Figure 2 shows the placement of thermocouples and CCAs in the three zones of the test room.

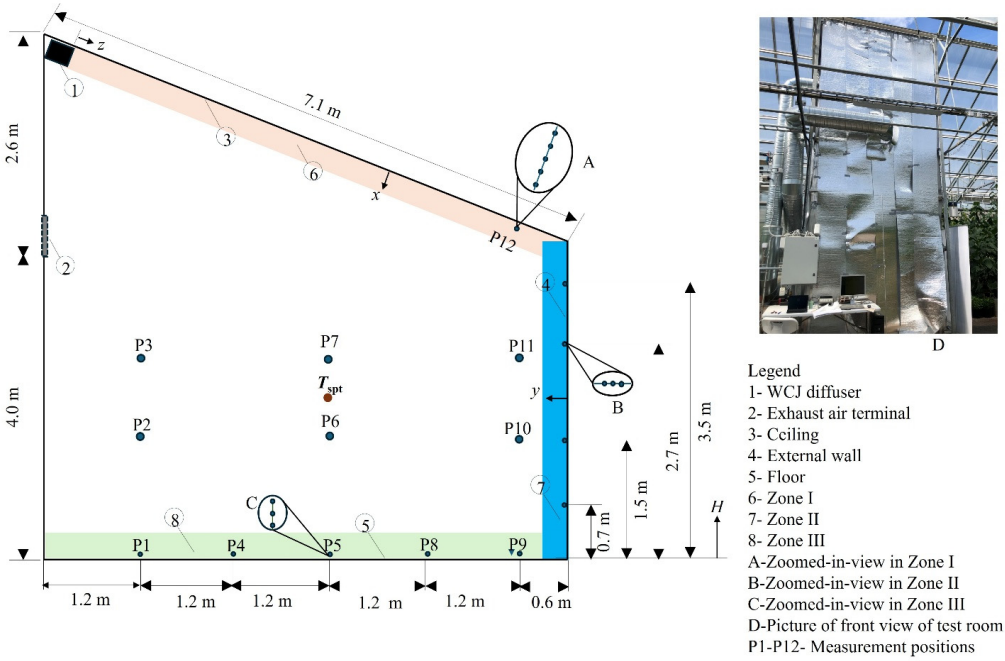


Figure 2. Side view of the test room illustrating WCJ velocity and temperature measurement zones, room air temperature measurement positions, and a front-view photo of the test room. Zoomed-in views (A, B, C) depict the orientation of constant current anemometers, while (D) shows the shaded side wall of the test room enclosed in the main greenhouse. Using constant current anemometers, the WCJ velocity and temperature measurement positions are marked as follows: H = 0.7 m, H = 1.5 m, H = 2.7 m, H = 3.5 m, P1, P4, P5, P8, P9, and P12. Room air temperature measurement positions, indicated as P2, P3, P6, P7, P10, and P11, with T_{spt} for the room air temperature setpoint.

In Zone I, CCAs measured air velocity and temperature in the boundary layer along the ceiling at P12, located at z = 6.0 m from the diffuser, using five sensors spaced 0.04 m apart, with perpendicular distances x ranging from 0.03 to 0.19 m from the ceiling surface. Zoomed-in view A in Figure 2 illustrates the spatial distribution of the CCAs at P12.

In Zone II, CCAs measured air velocity and temperature in the boundary layer along the inner surface of the vertical external wall at heights H = 0.7 m, 1.5 m, 2.7 m, and 3.5 m, using three sensors at each height, spaced 0.02 m apart, and positioned at y from 0.02 to 0.06 m. The zoomed-in view B in Figure 2 illustrates the orientation of the CCAs.

In Zone III, CCAs measured air velocity and temperature in the boundary layer along the floor at P1, P4, P5, P8, and P9, positioned at H of 0.05 m, 0.09 m, and 0.13 m above the floor. The zoomed-in view C in Figure 2 shows the spatial orientation of the CCAs in Zone III.

2.4.2. Temperature Measurements with Thermocouples

T-type thermocouples with a measurement range of −200 °C to 350 °C and an accuracy of ±0.5 °C were used to measure air and surface temperatures inside and outside the test

room. Selected for their thermal stability and suitability in low-to-moderate temperature environments [28], the thermocouples were interfaced with a 34972A LXI Agilent data acquisition system using LabVIEW 2017 for real-time data logging. Keysight Technologies, Inc., in Santa Clara, CA, USA manufactured this data logging equipment.

Thermocouples measured indoor air temperature at P2, P3, P6, P7, P10, and P11, while a PT100 sensor placed at H = 2 m in the room's center served as the T_{spt}; additional thermocouples measured the temperature of inlet air in the WCJ diffuser, exhaust air in the return duct, and outdoor air outside the main greenhouse. Ifm electronic GmbH, in Essen, Germany, manufactured the PT100 sensor used in the experiments. Furthermore, several thermocouples measured interior and exterior wall surface temperatures at H = 1.5 m and 2.5 m, ceiling temperatures along the WCJ flow from z = 0.0 to 1.0 m at 0.1 m intervals and from z = 1.0 to 6.0 m at 0.5 m intervals, the greenhouse roof surface at z = 6.0 m, and the floor surface temperature at 3.0 m from the external wall.

2.5. Solar Radiation Measurements with Pyranometers

The study used two Kipp & Zonen thermopile pyranometers to measure incident solar radiation on the greenhouse envelope, specifically the roof and external wall, in units of watts per square meter (W/m^2). Kipp & Zonen thermopile pyranometers were manufactured by Kipp & Zonen B.V., headquartered in Delft, the Netherlands. The pyranometers measure solar radiation in the spectral range of 280–2800 nm with a sensitivity of 4.56×10^{-6} $V/W{\cdot}m^2$ and $\pm 2\%$ accuracy for total daily radiation and are widely used in applications requiring high-fidelity data, such as solar energy studies, meteorology, and agriculture [29,30]. The pyranometers were connected to an Agilent 34972A LXI data acquisition unit via LabVIEW 2017, logging measurements at 60 s intervals to capture fluctuations due to variable sky conditions, such as intermittent cloud cover.

2.6. Approach and Analysis

The Black Box Heat Balance Model

The combined effects of solar radiation transmitted through the envelope, solar power absorbed and re-radiated by the floor, conductive heat exchange through the envelope surfaces, and convective cooling induced by the WCJ airflow impact the indoor air temperature. To characterize the indoor thermal conditions, the test room was analyzed using a black-box heat balance model, treating the system as a control volume defined by measurable heat inputs and outputs, while neglecting non-uniform flow fields, thermal stratification, dynamic moisture effects, and geometric complexities. This modeling approach is widely used in system-level thermal analyses, HVAC design, greenhouse temperature regulation, and building energy simulations, as it enables practical evaluation of overall energy performance when detailed environmental and flow data are unavailable [31]. This approach is suitable for this study because several parameters, such as humidity, wind speed, and radiative heat exchange, were not measured during the experiments. The experimenters established the test room's heat balance by quantifying indoor solar heat gains, heat exchange with the outdoor environment, WCJ-induced convective cooling, and conductive losses through the building envelope. The concrete floor acted as a thermal storage element, absorbing solar power during the day and releasing it gradually at night.

During the day, the test room gains heat through solar radiation, which heats the internal walls and the high-thermal-mass floor. Equation (1) expresses the total indoor solar heat gain ($P_{solar,transmitted}$) through the roof and external wall.

$$P_{solar,transmitted} = I_{roof} \cdot A_{roof} \cdot \tau_{roof} + I_{ext_wall} \cdot A_{ext_wall} \cdot \tau_{ext_wall} \quad (1)$$

where $P_{solar,transmitted}$ is the transmitted solar power [W], I_{roof} and I_{ext_wall} is solar radiation on the roof and external wall [W/m^2], respectively; A_{roof} is the roof area = 19.88 m^2, and A_{ext_wall} is the external wall area = 11.2 m^2, τ_{roof} and τ_{ext_wall} is the solar transmittance of the honeycomb polycarbonate envelope on the roof and external wall, respectively, determined using Fresnel and Beer-Lambert-Bouguer's laws that govern the reflection, transmission, absorption, and scattering of solar radiation through transparent materials. For double PC panels on a 26° sloped roof, τ_{roof} is estimated to be 0.55, and τ_{ext_wall} is 0.71 [32,33].

In an empty greenhouse, a substantial portion of the transmitted solar radiation is absorbed by the floor as formulated in Equation (2).

$$P_{floor,absorbed} = (I_{roof} \cdot A_{roof} \cdot \tau_{roof} \cdot F_{roof \to floor} + I_{ext_wall} \cdot A_{ext_wall} \cdot \tau_{ext_wall} \cdot F_{ext_wall \to floor}) \cdot \alpha_{floor} \quad (2)$$

where P_{floor}, absorbed is the absorbed solar power [W], $F_{roof \to floor}$ and $F_{ext_wall \to floor}$ are the view factors between the roof and the floor, and between the external wall and the floor, respectively. The $F_{roof \to floor}$ and $F_{ext_wall \to floor}$ are estimated at 0.78 and 0.34 [34], respectively. In an empty greenhouse with no obstructions and high sun altitude, a substantial portion of the solar power transmitted through the roof reaches the floor, thereby increasing the view factor. Still, because the sun is lower in the sky, some of the solar power transmitted through the external wall reaches the opposite wall, while the floor absorbs the rest. α_{floor} is the floor solar absorptance, estimated at 0.71 for concrete [35].

During the night, convective currents transfer heat from the warmer floor to the relatively cooler proximal room air, raising indoor air and surface temperatures. Equation (3) illustrates the convective heat transfer from the floor to the surrounding air in the room.

$$P_{floor,re-radiation} = h \cdot A_{floor} \cdot (T_{floor} - T_{flm}) \quad (3)$$

where $P_{floor,re\text{-}radiation}$ is power due to floor heat radiation [W]; h is the convective heat transfer coefficient [W/m^2·K], calculated from the Nusselt number for flows along a flat floor surface; T_{floor} is the floor surface temperature. Since $T_{floor} > T_{in}$ at night in summer, the study used the film temperature of the air in the boundary layer at the floor, $T_{flm} = (T_{floor} + T_{indoor})/2$. T_{indoor} is the indoor air in the room.

Assuming uniform solar heat absorption along the unobstructed floor, the study employed the convective heat transfer coefficient obtained by applying a constant heat flux over the floor surface, as per Equation (4).

$$h = \frac{\left(0.453 \cdot k \cdot Re_L^{\frac{1}{2}} \cdot pr^{\frac{1}{3}}\right)}{L} \quad (4)$$

where k is thermal conductivity [W/m·K], estimated at 0.026 for air between 14 and 25 °C [36]; L is the floor length, Re_L is the Reynolds number, and Pr is the Prandtl number, estimated at 0.7 [37].

To maintain the room air temperature at a setpoint, the WCJ is supplied at a lower temperature than ambient room air, allowing it to remove excess heat through convective cooling. Equation (5) provides the cooling power, contained in the WCJ, as a function of the mass flow rate and the temperature difference between the exhaust air (T_E) and the inlet air temperature (T_{in}).

$$P_{cool} = \dot{V} \cdot \rho \cdot C_p \cdot (T_E - T_{in}) \quad (5)$$

where P_{cool} is the WCJ cooling power [W], $\dot{V}$ is the volumetric airflow [m^3/s], ρ is the air density [kg/m^3], and C_p is the specific heat capacity [J/kg · K].

During the night, the WCJ provides passive heating because T_{in} is higher than T_E, so Equation (5) is replaced by Equation (6).

$$P_{heat} = \dot{V} \cdot \rho \cdot C_p \cdot (T_{in} - T_E) \quad (6)$$

Additionally, the greenhouse loses heat by conduction through the building envelope due to the temperature difference between the room air and the outdoor air. Equation (7) expresses the conductive heat transfer (P_{cond}) between the indoor and outdoor environments, principally through the roof and external wall. Although heat conduction through the side walls contributes negligibly, it is accounted for in Equation (7).

$$P_{cond} = U_{roof} \cdot A_{roof} \cdot \left(T_{ceiling} - T_{roof}\right) + U_{ext_wall} \cdot A_{ext_wall} \cdot (T_{ext_wall_inner} - T_{ext_wall_outer}) + \sum U_{sidewalls} \cdot A_{sidewall} \cdot (T_{sidewall_inner} - T_{sidewall_outer}) \quad (7)$$

where U_{roof}, U_{ext_wall} and $U_{sidewalls}$ are the U-values of the honeycomb polycarbonate on the roof, external wall and sidewalls [W/m^2.K], U_{roof} = 0.73 [W/m^2.K] because of two parallel PC films separated by a 0.05 m air gap; U_{ext_wall} = $U_{sidewalls}$ = 1.95 [W/m^2.K], $T_{ceiling}$ is the ceiling surface temperature [°C], T_{roof} is the roof surface temperature [°C], $T_{ext_wall_inner}$ and $T_{ext_wall_outer}$ are the surface temperatures on the inner and exterior of the external walls [°C], respectively; $A_{sidewall}$ $T_{sidewall_inner}$, $T_{sidewall_outer}$ is area [m^2], inner surface temperature [°C] and outer surface temperature of shaded sidewalls [°C], respectively.

The net power (P_{net}) results from the summation of significant indoor greenhouse heat gains, heat removal, and losses from various heat transfer mechanisms, as illustrated in Equations (1)–(7). Equation (8) illustrates the general net power in the greenhouse.

$$P_{net} = P_{solar,transmitted} + P_{floor,re-radiation} - P_{cool} - P_{floor,absorbed} - P_{cond,roof} - P_{cond,ext_wall} - P_{cond,sidewalls} \quad (8)$$

During the day, the floor absorbs the incident solar radiation, and the outer surfaces become warmer than the interior surfaces, driving heat conduction from outdoors into the interior. Under these conditions, Equation (8) transforms into Equation (9):

$$P_{net} = P_{solar,transmitted} + P_{cond,roof} + P_{cond,ext_wall} + P_{cond,sidewalls} - P_{cool} - P_{floor,absorbed} \quad (9)$$

At night, in the absence of solar radiation, the floor releases stored heat by re-radiation, while the WCJ system provides heating to maintain the indoor temperature. The cooler outdoor air reduces the outer-surface temperature, thereby driving heat transfer from the test room to the environment. Substituting Equation (5) with Equation (6) in Equation (8) and removing non-contributing terms yields Equation (10):

$$P_{net} = P_{heat} + P_{floor,re-radiation} - P_{cond,roof} - P_{cond,ext_wall} - P_{cond,sidewalls} \quad (10)$$

P_{net} quantifies the balance among solar transmission, floor heat absorption, WCJ convective cooling, floor-to-jet convective exchange, and conductive transfer through the roof and external wall glazing. It denotes the power required to sustain the target indoor air temperature in the greenhouse. When $P_{net} > 0$, solar gains exceed WCJ cooling, causing the room temperature to rise above T_{spt}. When $P_{net} < 0$, conductive losses exceed WCJ heating and floor release, typically at night, lowering the room temperature below T_{spt} and necessitating a higher supply air temperature or supplementary heating. At $P_{net} = 0$, the system achieves an instantaneous power balance. Assuming adequate cooling capacity and perfect energy balance in the greenhouse, the indoor air temperature (T_{indoor}) can be

determined by equating the WCJ's convective cooling power to the net power as formulated in Equations (11) and (12):

$$P_{\text{net}} = \rho \cdot \dot{V} \cdot C_p \cdot (T_{\text{indoor}} - T_{\text{in}}) \quad (11)$$

Rearranging gives the indoor air temperature in Equation (11)

$$T_{\text{indoor}} = \frac{P_{\text{net}}}{\left(\rho \cdot \dot{V} \cdot C_{\text{p}}\right)} + T_{\text{in}} \quad (12)$$

3. Results and Discussion

This section presents the results and discussion of an investigation into the thermal performance of a WCJ system for climate regulation under varying outdoor temperatures and solar radiation in the test room described in Section 2.1. The analysis demonstrates that various factors, including room air temperature setpoints (T_{spt}), the number of nozzle rows (n), and external wall shading, influence system behavior and overall thermal performance.

3.1. Solar Radiation and Outdoor Air Temperature

In summer, high solar irradiance and outdoor air temperatures increase the indoor air temperatures by transmitting significant solar energy through the building envelope. Figure 3 shows the external climate drivers measured during the experimental period, including incident solar radiation on the greenhouse roof and the external wall, as well as outdoor air temperature, for representative summer and autumn runs. These boundary conditions define the primary external loads on the greenhouse's thermal balance and provide essential context for interpreting observed variations in room air temperature, supply air temperature, and net power across different operational settings of the WCJ system. Figure 3a–d shows the diurnal evolution of solar radiation incident on the greenhouse roof (I_{roof}) and external wall ($I_{\text{ext_wall}}$) during summer and autumn. Figure 3e,f show outdoor air temperatures during summer and autumn, respectively.

Peak incident radiation on the roof in summer reached approximately 1000 W/m^2, while the autumn peak was 700 W/m^2, representing a seasonal reduction of up to 30%. Similarly, incident solar radiation on the external wall reached approximately 800 W/m^2 in summer, compared with 500 W/m^2 in autumn (a 40% decrease). This seasonal decline reflects reduced solar elevation and a shorter photo-period in autumn. The seasonal shift in outdoor air temperature mirrors this trend: summer maxima exceeded 30 °C, while autumn maxima remained below 22 °C, resulting in a 35% reduction in daytime peak values. Summer ambient climatic conditions produced up to 30% greater solar gains and outdoor temperatures 10 °C higher than in autumn, resulting in substantially increased indoor cooling demand.

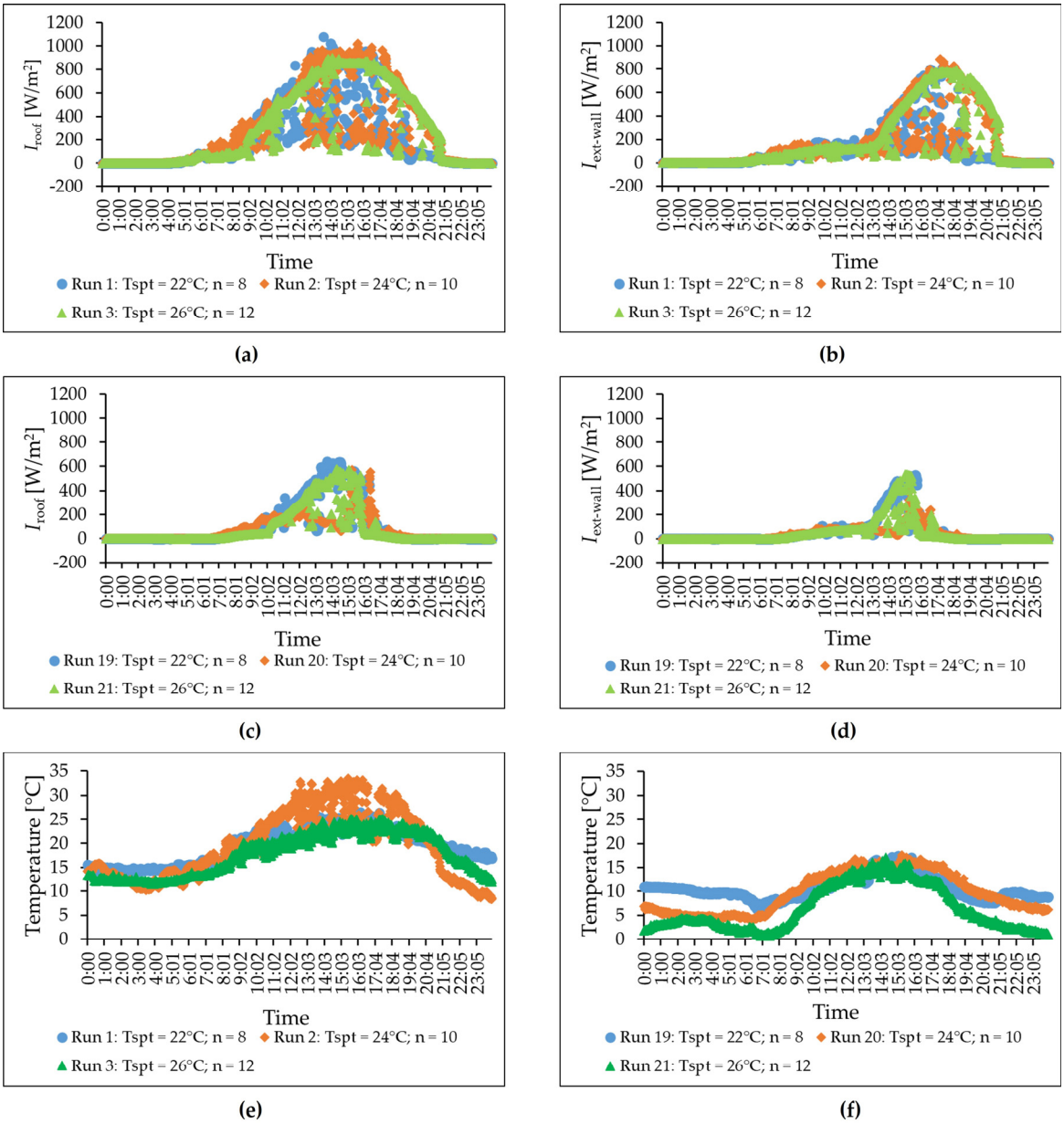


Figure 3. Time-series of external climate conditions during selected experimental runs: (**a**) incident solar radiation on the roof in summer, (**b**) incident solar radiation on the external wall in summer, (**c**) incident solar radiation on the roof in autumn, (**d**) incident solar radiation on the external wall in autumn, (**e**) outdoor air temperature in summer, and (**f**) outdoor air temperature in autumn.

3.2. WCJ Velocity

Figure 4 illustrates the magnitude and spatial distribution of WCJ velocity along the Ceiling at P12, external wall at H = 2.7 m, and floor at P1, P4, P5, and P8 during summer and autumn. The results highlight how different setpoint temperatures and nozzle configurations influence the airflow trajectory and velocity decay, thereby characterizing the momentum transport and mixing efficiency of the WCJ system within the greenhouse. Figure 4a,c,e illustrate air velocity for runs at T_{spt} = 22 °C, 24 °C, and 26 °C, respectively. Figure 4b,d,f illustrate the spatial distribution of velocity along the ceiling (P12), external wall (H = 2.7 m), and floor (P5), respectively, for run 2.

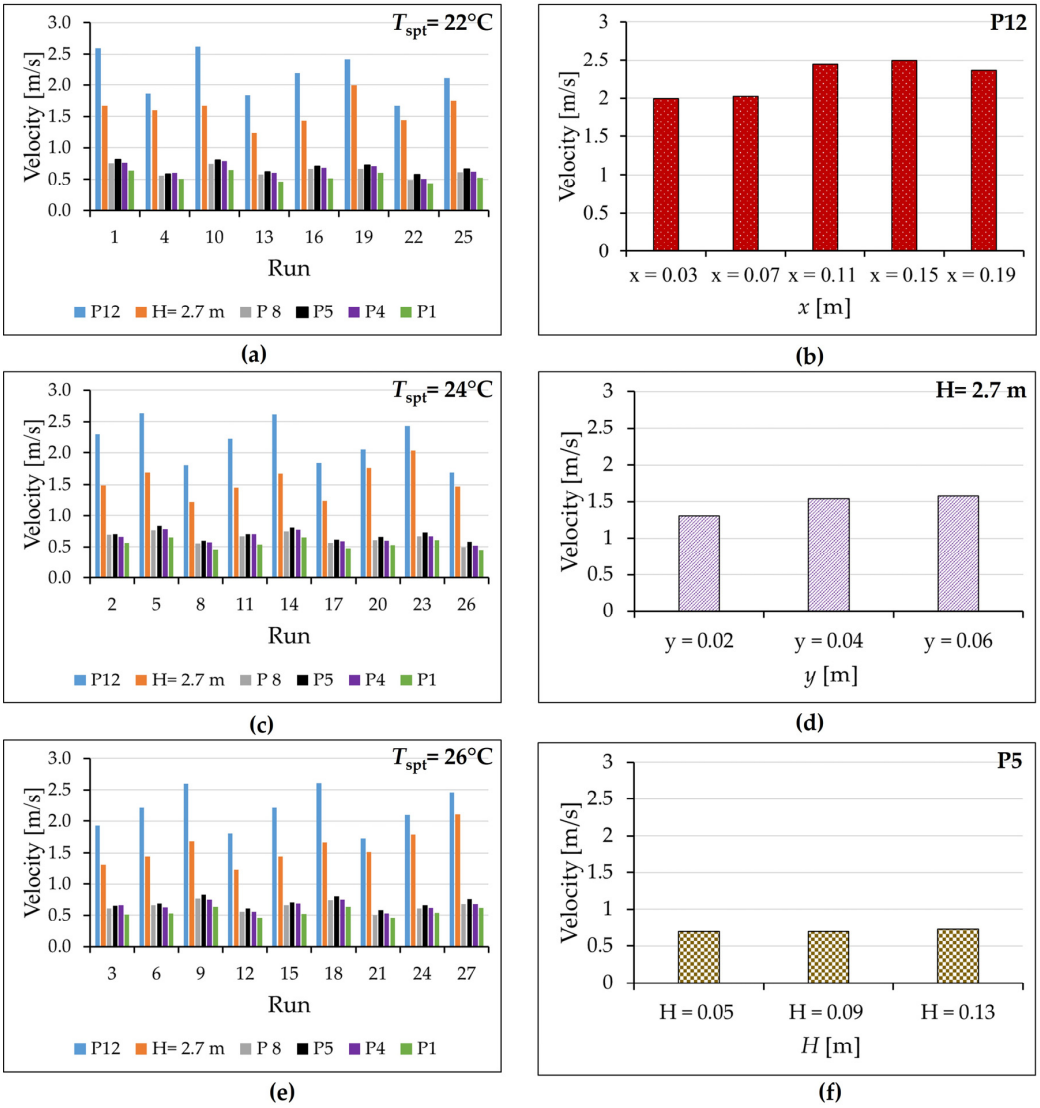


Figure 4. Wall confluent jets (WCJ) velocity along the ceiling (P12), external wall (H = 2.7 m), and floor positions (P1, P4, P5, and P8) in summer and autumn: (**a**) WCJ velocity with runs at T_{spt} = 22 °C (**b**) WCJ velocity distribution in the boundary layer in Zone I at P12, (**c**) WCJ velocity with runs at T_{spt} = 24 °C, (**d**) WCJ velocity distribution in the boundary layer Zone II at H = 2.7 m, and (**e**) WCJ velocity with runs at T_{spt} = 26 °C, and (**f**) WCJ velocity distribution in the boundary layer in Zone III at P5. Note: *x*, *y* and *H* are the perpendicular distances from the ceiling, inner surface of the external wall and the floor into the room, respectively.

Across all runs, the results demonstrate that WCJ velocity generally decays with distance from the diffuser, with higher velocities sustained near the ceiling (P12, over 2.0 m/s) and progressively lower values measured along the external wall (H = 2.7 m, about 1.4 m/s) and at the floor (P1, P4, P5, and P8, lowest velocities of 0.4–0.9 m/s) accounting for up to 70% decay in streamwise velocity. This trend reflects the effects of friction, momentum dissipation, and enhanced mixing with room air. This result confirms the classical turbulent-jet theory, which predicts rapid axial decay of the centerline velocity and an increase in the jet width. Across all runs, the velocities in Zone III remain uniform and fall within the acceptable range for diverse greenhouse crops [24], supporting adequate air circulation and thermal energy exchange. Increasing *n* at a constant total airflow reduced core velocities by 10–25% at P12, but also reduced downstream velocity decay, as indicated by a minimal velocity magnitude difference compared to runs at lower *n*. Velocities in Zone III show negligible reductions due to the greater shielding from higher *n*, which reduces entrainment and slows velocity

decay along the ceiling and external wall. Greenhouse operators can optimize performance by using a higher n to ensure uniform crop microclimates. However, excessively larger n may necessitate higher airflow rates to maintain adequate air movement in Zone III, creating a trade-off between fan and cooling energy use.

Seasonal effects were minor, with autumn runs showing 8% lower velocities than summer runs due to density differences. External wall shading and T_{spt} adjustments produced negligible changes (<5%) in the measured velocity field, confirming that these variables primarily affect thermal boundaries rather than momentum distribution. Comparing run 1 with run 5, and run 2 with run 6, shows that T_{spt} has a marginal effect on WCJ velocity. Figure 4b,d,f show that the velocity increases away from the surfaces, a characteristic behavior in boundary layers.

3.3. WCJ Temperature

The air temperature in the boundary layers reflects an interplay of the inlet air temperature, convective heat exchange with room air and interior surfaces, and heat gains from the external environment. Air velocity is the primary convective transport mechanism governing sensible heat removal and establishing the desired thermal environment within the greenhouse. Figure 5a,c,e depict the spatial evolution of air temperature across the ceiling, wall, and floor zones under different setpoints and seasonal conditions. Figure 5b,d,f show the spatial temperature distribution in the three zones for Run 2.

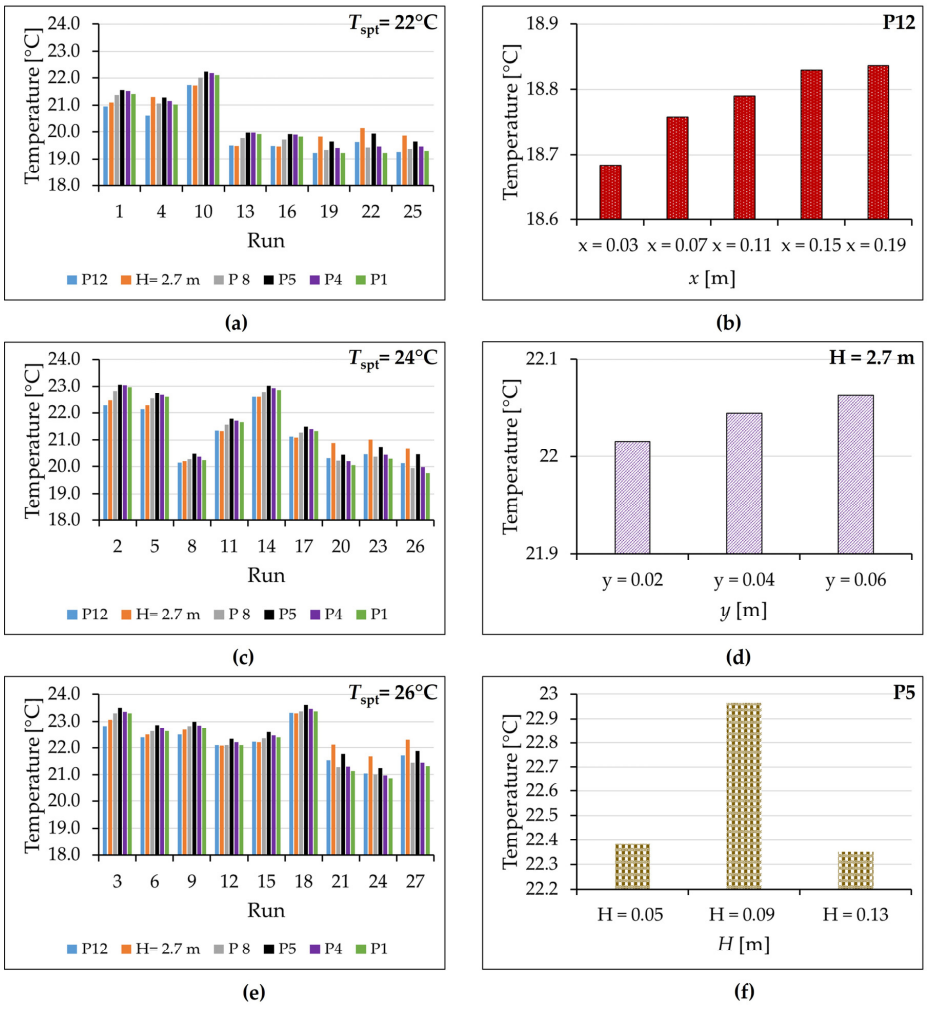


Figure 5. Wall confluent jet temperature in Zone I at P12, Zone II at H = 2.7 m, and Zone II at P1, P4, P5, and P8 in summer and autumn. (**a**) WCJ temperature with runs at T_{spt} = 22 °C, (**b**) WCJ

temperature distribution in the boundary layer in Zone I at P12, (**c**) WCJ temperature with runs at T_{spt} = 24 °C, (**d**) WCJ temperature distribution in the boundary layer in Zone II at H = 2.7 m, and (**e**) WCJ temperature with runs at T_{spt} = 26 °C, and (**f**) WCJ temperature distribution in the boundary layer in Zone III at P5. Note *x*, *y*, and *H* are the perpendicular distances from the ceiling, inner surface of the external wall, and the floor into the room, respectively.

The results indicate a progressive rise in air temperature from the ceiling to the floor due to entrainment and heat exchange, with ceiling-to-floor warming ranging from approximately 0.8 to 1 °C in summer and 0.4 °C in autumn for runs with an unshaded external wall. The WCJ temperature remained relatively uniform in Zone III, with variations limited to ±3%. Seasonal conditions exerted the strongest influence, reducing WCJ temperatures by up to 10% due to the dominant effect of outdoor air conditions. External wall shading moderates WCJ temperature increases by 4–6% through reduced conductive heat transfer. By limiting wall heat flux, shading decreases Zone II temperatures, reduces downstream jet warming, and flattens temperature profiles across the zones. Raising the T_{spt} increased WCJ temperature by up to 8%, effectively reducing cooling demand for a given indoor climate target. At higher T_{spt}, higher inlet air temperatures apply, reducing the temperature gradient between the WCJ and the surrounding air and thereby decreasing buoyancy-driven mixing. Increasing the *n* enhanced temperature uniformity and limited the mean WCJ temperature rise by 2–4%. Increasing *n* tends to lower the WCJ temperature by improving momentum conservation, thereby increasing cooling capacity.

Figure 5b,d,f show that the temperature increases with distance from the surface, indicating the WCJ's ability to transport heat from the surface. However, the air temperature decreases above the floor beyond H = 0.09 m as the cooler WCJ mixes with the surrounding air, thereby lowering the room air temperature to track the T_{spt}.

3.4. Surface Temperatures

The cold air layers flowing proximally to the surfaces facilitate heat removal by increasing local convective heat transfer, thereby reducing surface temperature.

3.4.1. Ceiling and External Wall's Inner Surface Temperature

Intensive shortwave solar radiation transmitted through the polycarbonate envelopes elevates the ceiling and external wall surface temperatures. Figure 6 shows the measured ceiling surface temperatures (a), (c), and (e), and the inner surface temperatures of the external wall (b), (d), and (f) under different T_{spt} and *n*. These results provide insight into how cold WCJ flow behavior influences heat transfer at interior envelope surfaces.

For the same T_{spt} and *n*, runs conducted in summer exhibit higher external wall and ceiling temperatures than those performed in autumn, with the difference being more pronounced for the external wall. Seasonal climatic conditions, such as higher solar load and higher outdoor temperatures in summer, increase heat gain through the greenhouse envelope and elevate the surface temperatures. Consequently, external wall surface temperatures are up to 25% higher, and ceiling surface temperatures are up to 10% higher, in summer than in autumn. Across most runs, external wall surface temperatures were marginally (<5%) higher than those of the ceiling. Runs 1 and 4 show that lower T_{spt} reduced ceiling temperatures by increasing the thermal gradient between the cooler WCJ supply air and the warmer ceiling surface.

Shading lowers median ceiling surface temperatures by up to 10% and decreases the internal surface temperatures of the external wall by 10–30%. Shading decreases incident solar radiation and therefore reduces the absorbed solar heat on the external wall; this lowers the wall surface temperature directly and reduces radiative and convective heat input to the interior, which in turn reduces the ceiling temperature to a lesser degree.

However, shading limits the incident solar radiation needed for photosynthesis; while it benefits light-saturated crops in hot climates by reducing heat stress and water demand, it may lower yields for light-limited crops, making adaptive shading systems essential to match crops and seasonal needs.

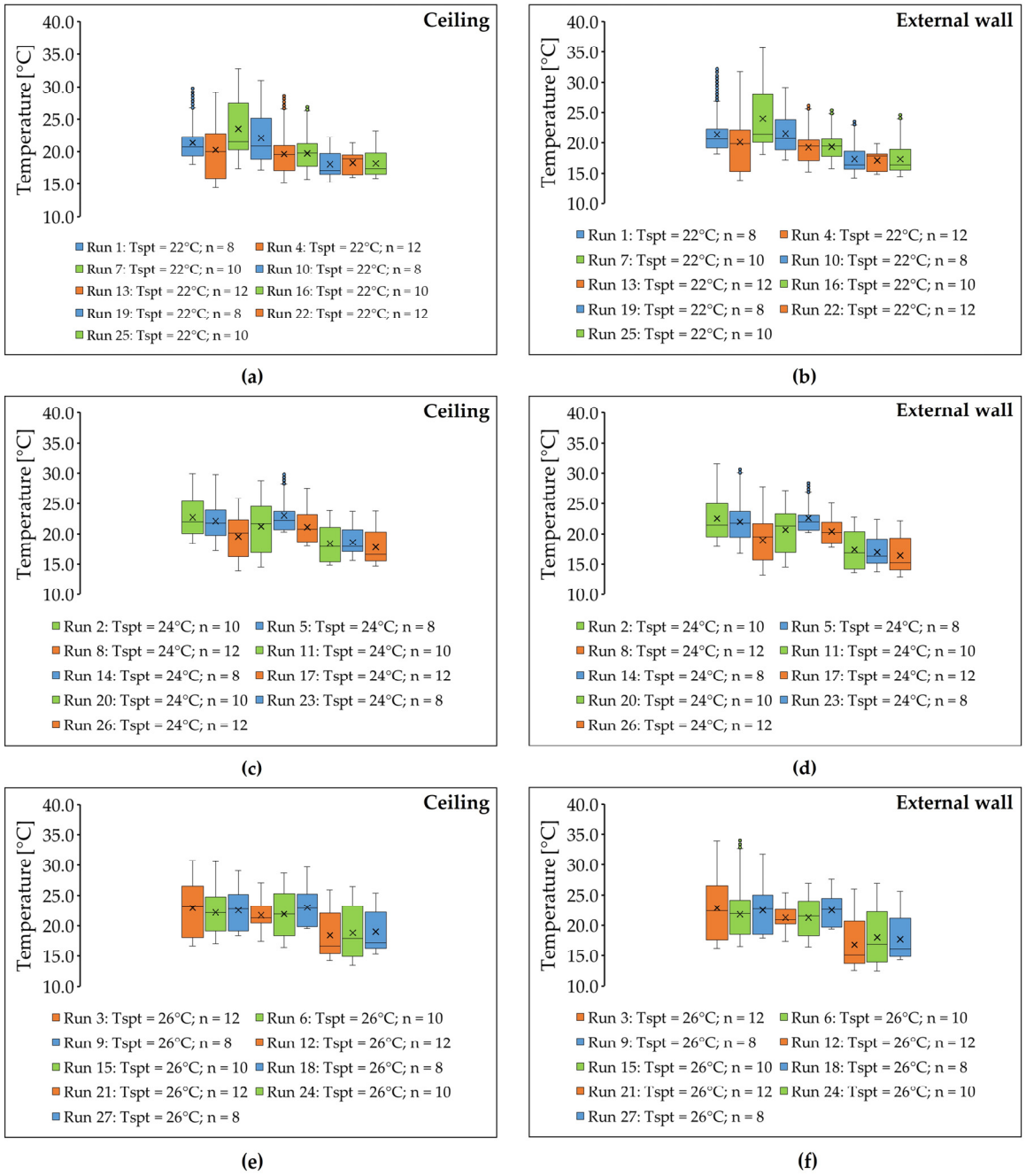


Figure 6. Ceiling surface temperature and inner surface temperature of external wall: (**a**) ceiling surface temperature for runs at T_{spt} = 22 °C, (**b**) inner surface temperature of external wall for runs at T_{spt} = 22 °C, (**c**) ceiling surface temperature for runs at T_{spt} = 24 °C, (**d**) inner surface temperature of external wall for runs at T_{spt} = 24 °C, (**e**) ceiling surface temperature for runs at T_{spt} = 26 °C, and (**f**) inner surface temperature of external wall for runs at T_{spt} = 26 °C. Note that blue represents runs with n = 8, green represents runs with n = 10, and orange represents runs with n = 12.

Runs with larger n show lower median ceiling and wall surface temperatures and smaller scatter than runs with fewer nozzle rows at the same T_{spt}. The effect is most pronounced on the ceiling where the WCJ is attached, and slightly less pronounced on

the external wall. Increasing n reduced the ceiling and wall surface temperatures by up to 8% because broader, lower-momentum jets promote uniform advection over surfaces, reducing localized hot spots and lowering the median surface temperature by increasing surface cooling uniformity. WCJ configuration affects how efficiently the jets remove heat from the ceiling/wall surfaces. At a constant total airflow rate, increasing n reduces the nozzle exit velocity and enhances jet spread and surface attachment, resulting in a broader, more stable WCJ. Runs combining lower T_{spt} with higher n (e.g., 4, 13, and 22) exhibited greater ceiling cooling stability, while intensified wall cooling reflected the development of a high-momentum convective boundary layer consistent with wall-jet heat transfer theory.

Increasing T_{spt} raises the ceiling and inner external wall surface temperatures by up to 17% and 20%, respectively. Raising T_{spt} changes the mean indoor air temperature and the convective heat transfer between the room air and surrounding surfaces. Surfaces in contact with the WCJ boundary layer experience higher convective heat fluxes when the air is warmer, so surface temperatures tend to track changes in bulk air temperature. Thus, a higher T_{spt} increases indoor temperatures and reduces the driving thermal gradient for heat dissipation, resulting in warmer surfaces. The external wall was more responsive than the ceiling due to the longer distance from the diffuser. This thermal behavior aligns with previous studies, which indicate that temperature setpoint control is a critical determinant of greenhouse microclimate and cooling demand [38].

3.4.2. Floor Surface Temperature

The measured floor surface temperatures under different T_{spt} and n provide insight into how the WCJ cooling system influences the thermal conditions at the crop-ground interface (soil temperature). Since the floor acts as both a thermal sink and a source of radiative exchange with the canopy, these results are critical for Figure 7a–c illustrate the variations in floor surface temperature over 24 h at T_{spt} = 22 °C, 24 °C, and 26 °C, respectively.

Across the runs, floor surface temperatures increased by approximately 10–16% with an increase in T_{spt}. The floor absorbs a significant portion of solar radiation transmitted through the envelopes, raising its surface temperature. Floor surface temperature variations were less pronounced than those observed on ceiling or external wall surfaces, due to the thermal damping effect of the floor mass. Stable and uniform floor temperatures are critical for maintaining favorable root-zone and near-canopy microclimates, thereby reducing localized overheating, minimizing crop heat stress, and supporting consistent growth and transpiration patterns.

Increasing the n lowered floor surface temperatures and variability by approximately 6%. Runs 4, 13, and 22, combined lower T_{spt} with higher n to produce cooler and more uniform floor temperatures. The narrower interquartile ranges observed at higher n further demonstrate that enhanced air mixing in the lower parts of the occupied zone reduces stratification and localized hot spots, resulting in more uniform plant-level thermal conditions. Among the tested configurations, the combination of moderate T_{spt}, higher n, and external wall shading proved most effective at stabilizing floor-surface temperatures while reducing cooling energy demand.

External wall shading lowered floor surface temperatures by 6–12%, with greater daytime effects and smaller nighttime reductions. This thermal behavior demonstrates that shading primarily attenuates solar and conductive heat gains, thereby limiting secondary heating of the floor. Seasonal contrasts reinforced this effect: in autumn, reduced outdoor air temperatures and solar loading resulted in floor surface temperatures up to 20% lower than in unshaded summer scenarios. Under these conditions, the WCJ cooling system demonstrated its ability to maintain the recommended soil temperature threshold for greenhouse crops, such as tomatoes [13].

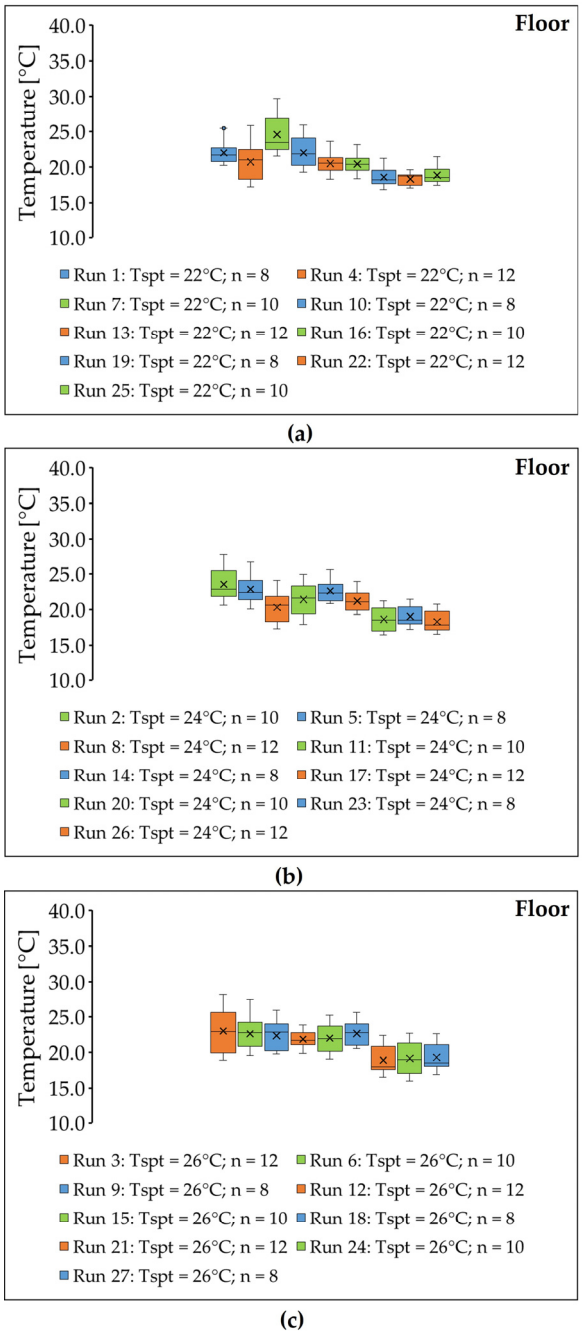


Figure 7. Floor surface temperature: (**a**) for runs with T_{spt} = 22 °C, (**b**) for runs with T_{spt} = 24 °C, and (**c**) for runs with T_{spt} = 26 °C. Note that blue represents runs with n = 8, green represents runs with n = 10, and orange represents runs with n = 12.

The results highlight the floor's role as a thermal buffer within the greenhouse. During midday, the floor absorbed a substantial share of transmitted solar radiation, storing it as thermal mass and thereby preventing excessive temperature increases at the ceiling and external walls. At night, it gradually released the stored heat, maintaining indoor air, ceiling and external wall temperatures. The result reinforces a previous study that demonstrated the impact of concrete floors on greenhouse microclimates [39].

3.5. Inlet Air Temperature

The AHU dynamically adjusted the WCJ inlet air temperature (T_{in}) through its cooling coil to offset solar and outdoor heat gains, thereby maintaining the target T_{spt}. Figure 8 illustrates the variation in inlet air temperature across different experimental conditions,

highlighting the combined effects of T_{spt}, n, and external wall shading boundary conditions. These results provide a basis for understanding how WCJ inlet air responds to external thermal loads, thereby shaping the cooling effectiveness and overall energy performance of the greenhouse. The sub-figures distinguish the effects of Figure 8a–c varying T_{spt} under constant nozzle configuration in summer and autumn, and Figure 8d changes in n during summer, thereby enabling assessment of how control variables and boundary conditions shape inlet air temperature behavior in the greenhouse.

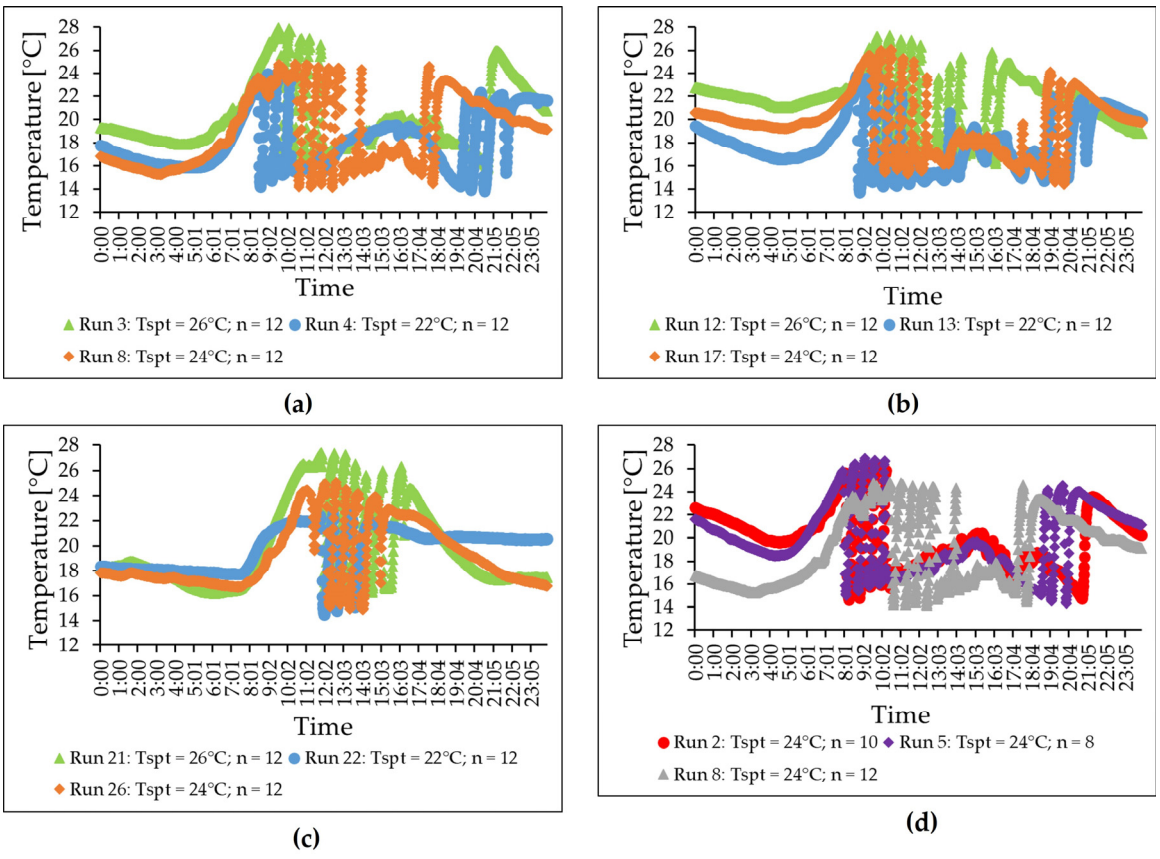


Figure 8. Variation in inlet air temperature under different experimental conditions: (**a**), influence of room air temperature setpoint (T_{spt}) in summer at n = 12 with unshaded external wall, (**b**), influence of room air temperature setpoint (T_{spt}) in summer at n = 12 with shaded external wall, (**c**), influence of room air temperature setpoint (T_{spt}) in autumn at n = 12 with unshaded external wall, (**d**) effect of number of nozzle rows in summer at T_{spt} = 24 °C.

The inlet-air temperature shows a clear diurnal pattern and a strong dependence on T_{spt} and seasonal boundary conditions. During high-insolation periods (afternoon), the inlet temperature lies near the lower bound of the temperature range (≈14 °C). In contrast, during midmorning and evening under mild solar irradiance, the inlet air exhibits transient oscillations between 14 °C and 26 °C due to intermittent WCJ cooling. At night, it fluctuates around room temperature.

Raising the T_{spt} increases daytime inlet temperatures by approximately 15%, with the largest rise occurring at midday, when the controller permits warmer room air, and the WCJ inflow equilibrates to the higher indoor air temperature target. A higher T_{spt} reduces the required inlet-to-room temperature difference by decreasing the controller's demand for cold inlet air, allowing the system to deliver warmer inlet air at a lower cooling intensity. T_{spt} is the dominant factor influencing the inlet temperature, with a 2 °C increase resulting in an 8–11% rise.

Increasing the n decreases the peak daytime inlet temperature by 4–10%. Increasing n for a fixed total flow reduces the pressure drop in the diffuser, resulting in lower frictional heat generation at the diffuser and nozzle outlets and, in turn, lower temperatures. This result suggests that WCJ diffuser designers and greenhouse operators should treat nozzle count and layout as variables that can be controlled rather than fixed hardware. Staging nozzles (by changing the number of active rows or modulating which rows operate) can be used in combination with T_{spt} and shading to optimize inlet air temperature, meeting diverse microclimate needs at low energy use.

Runs conducted in autumn demonstrate that shorter cooling periods, during which the WCJ system intermittently cools the inlet air to maintain the T_{spt}. The WCJ cooling system does not require active, intensive cooling because intermittent cooling causes the inlet air temperature to oscillate between 16 °C and 26 °C during the day, thereby reducing cooling energy use

External wall shading reduces shortwave radiation transmission through the polycarbonate, lowering midday solar gains and instantaneous cooling demand, thereby increasing the inlet air temperature by about 5–12%. However, increasing the T_{spt} raises the inlet air temperature, indicating that shading moderates but does not eliminate the setpoint's influence. Shading is a passive, complementary strategy that can be integrated into the WCJ cooling system to enhance thermal performance. Moreover, coupling WCJ cooling systems with absorption chillers that use waste heat, such as excess industrial heat (e.g., nearby steel plant producing 100–650 °C waste heat), combined heat and power [40], data centers [41], and waste-to-energy systems (e.g., biogas) [42] offers a sustainable pathway to harness cooling energy for greenhouse operation. By utilizing waste heat from various sources, the WCJ cooling system decreases primary energy use and associated greenhouse gas emissions, thereby mitigating climate change. Employing low-exergy heat for space cooling conserves high-exergy electricity for essential applications, such as lighting, appliances, and industrial operations, enhancing energy access and supporting Sustainable Development Goal 7, which aims to achieve affordable and clean energy.

3.6. Indoor Air Temperature

The WCJ cooling system offsets solar heat gains to create an acceptable indoor thermal environment, as specified by the T_{spt}. Figure 9 illustrates the variation in indoor air temperature across different experimental conditions, highlighting: Figure 9a the effects of T_{spt} for unshaded external wall in summer and Figure 9b the effects of T_{spt} with shaded external wall in summer, Figure 9c the effects of T_{spt} for unshaded external wall in autumn, Figure 9d effects of n in autumn on the greenhouse's thermal environment.

All runs exhibit an apparent diurnal variation, with the lowest temperatures occurring during the night/early morning (approximately 14 °C) and the highest temperatures in the afternoon (28 °C). Daytime solar peaks occasionally drove room air temperature above the setpoint because the cooling system could not immediately counter rapid solar gains due to a response lag and limited installed cooling capacity. Deviations also occurred on autumn nights when the indoor temperature dipped below the T_{spt} due to the non-availability of active heating. However, the WCJ cooling system maintained indoor air temperatures within ±1.5 °C of T_{spt} for most runs under daytime summer and autumn conditions. Further analysis of the heat-removal effectiveness index showed that the values approached unity, indicating a uniform distribution of room air temperature.

Raising T_{spt} elevates the indoor temperature, with a 4 °C increase yielding about 20–25% higher room air temperatures at constant n and season. While higher T_{spt} lowers cooling demand and peak loads, it may compromise heat-sensitive crops. In contrast, modest reductions (2–4 °C) reduce peak stress hours but require greater cooling effort to

offset the resultant huge cooling demand. Growers should therefore set T_{spt} at the lowest acceptable crop tolerance to balance energy savings with crop protection.

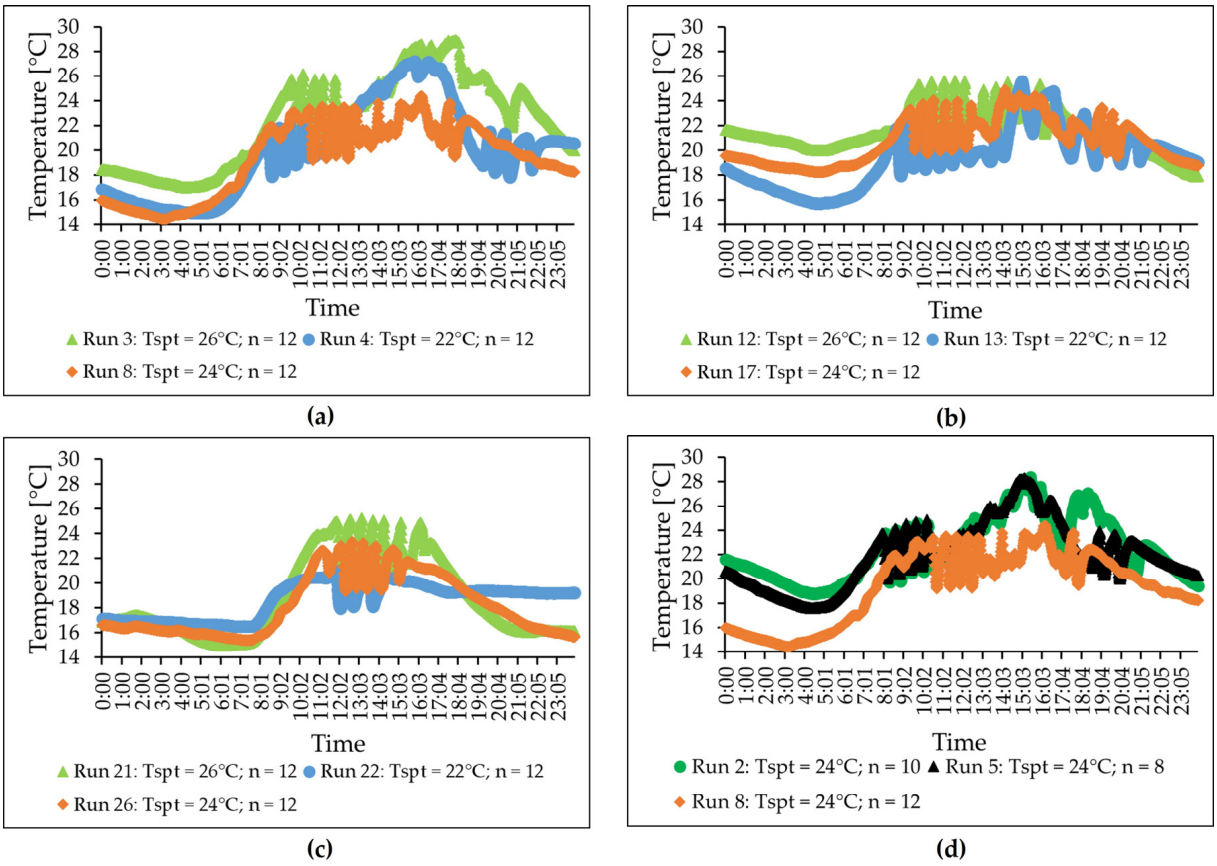


Figure 9. Variation in room air temperature: (**a**), influence of room air temperature setpoint (T_{spt}) in summer at n = 12 with unshaded external wall, (**b**), influence of room air temperature setpoint (T_{spt}) in summer at n = 12 with shaded external wall, (**c**), influence of room air temperature setpoint (T_{spt}) in autumn at n = 12 with unshaded external wall, (**d**) effect of number of nozzle rows in summer at T_{spt} = 24 °C.

At constant season and T_{spt}, increasing n enhanced convective heat removal and mixing in the occupied zone, lowering peak temperatures by 2–6% and improving local thermal homogeneity. Changing n at a constant total volumetric flow rate alters individual jet velocities and their interactions with the ceiling/wall boundary layers. These flow changes alter entrainment, mixing, and local convective heat transfer to the envelope and floor. Raising n primarily reduces flow recirculation and spatial variability in the near field, thereby enhancing the jet's cooling efficiency and improving heat removal near the crop level in the far field. For heat-sensitive crops, this improved microclimate uniformity is often more critical than a reduction in mean temperature, as localized hotspots can still impair growth [24].

External wall shading reduced midday peak indoor air temperatures by up to 35% and the mean indoor temperature by approximately 5–15% (depending on the time of day and irradiance). Therefore, shading lowers instantaneous cooling demand during high-sun periods and flattens diurnal swings, thereby stabilizing the greenhouse thermal environment. By limiting conductive and solar heat gains, shading decreased peak cooling capacity requirements and lowered peak temperatures and temperature variability, but extended the active cooling system's run-time, as demonstrated in Run 17 compared to Run 8. These results align with prior greenhouse studies, which report that external shading or

thermal screens reduce peak temperatures by several degrees and significantly cut cooling loads [43]. Integrating shading with WCJ cooling demonstrates that adaptive strategies, such as real-time airflow modulation, hybrid ventilation, and low-transmittance glazing, can enhance performance and reduce energy use.

In autumn, reduced outdoor temperatures and solar radiation lower internal heat gains and cooling demand, enabling the WCJ system to operate at partial load or intermittently shut down. Compared to summer under similar T_{spt} and n, daytime peak temperatures drop by up to 30%, and mean room temperatures are closer to the setpoint. Indoor temperatures remained within acceptable thresholds for greenhouse crops [25], indicating that minimal space heating during transitional seasons (spring and autumn) reduces energy use while maintaining a suitable growing environment. These results, together with those reported in [23], suggest that the growing period can be extended throughout the year for a greenhouse using WCJ cooling and heating systems.

3.7. Power Balance

Figure 10 shows the temporal variation of the net power (P_{net}) for selected experimental runs, illustrating the influence of T_{spt}, n, and the external wall shading on the greenhouse's power balance. The subfigures isolate specific effects: Figures 10a and 10b show the effect of T_{spt} under a constant number of nozzle rows in summer conditions under unshaded and shaded external walls, respectively; Figures 10c and 10d examine the effect of n on the net power in summer and autumn, respectively, with the greenhouse's external wall unshaded.

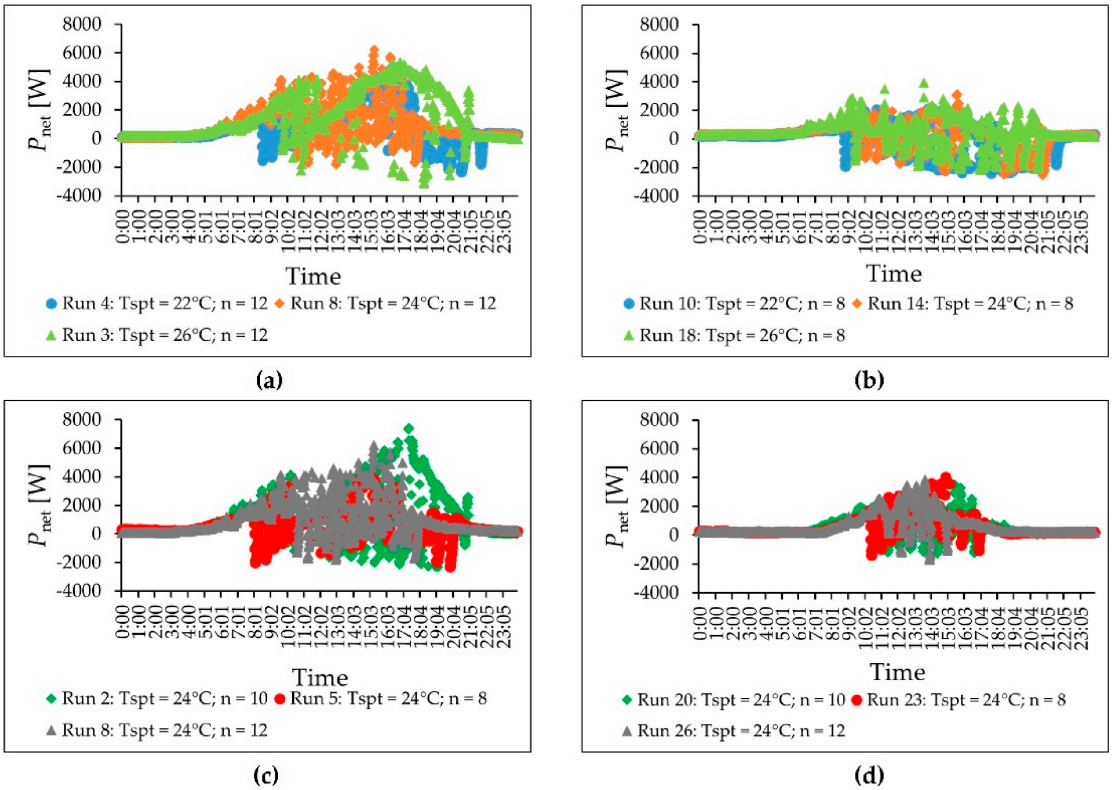


Figure 10. Temporal variation of the net power (P_{net}) under different experimental conditions: (**a**) effect of room air temperature setpoint (T_{spt}) in summer with a constant number of nozzle rows (n) and an unshaded external wall, (**b**) effect of room air temperature setpoint (T_{spt}) in summer with a constant number of nozzle rows (n) and a shaded external wall, (**c**) effect of number of nozzle rows in summer with unshaded external wall at fixed T_{spt}, (**d**) effect of number of nozzle rows in autumn with unshaded external wall at fixed T_{spt}.

Summer runs exhibited higher net power, with midday peaks of up to 6 kW driven by intense solar radiation and warmer outdoor conditions. In autumn, the peak net power drops below 4 kW, enabling the WCJ system to maintain thermal balance with reduced energy use. This reduction is attributed to lower outdoor air and surface temperatures and weaker solar radiation, which together increase the convective cooling efficiency of the WCJ.

P_{net} increased with higher T_{spt} due to warmer indoor air and exhaust air, resulting from reduced ventilation cooling effectiveness, which allowed 20–40% more net power depending on the time of day and external solar load. Increasing T_{spt} reduced the room air-jet temperature gradient, diminishing buoyancy-driven flow entrainment and heat transfer. Consequently, the net heat stored in the air and structural surfaces increases, leading to a higher P_{net}. Predominant solar gains prevent the WCJ cooling system from fully offsetting thermal loads unless operators increase the airflow rate or implement additional cooling strategies. These results confirm that T_{spt} selection directly influences greenhouse thermal balance and crop exposure, consistent with previous studies [12]. Greenhouse growers may choose a slightly higher T_{spt} (within crop tolerance) to reduce cooling energy use and costs.

Increasing the n enlarged the effective diffusion area and promoted the smoother merging of the confluent jets, thereby enhancing airflow uniformity and improving convective heat removal throughout the greenhouse. The additional nozzle rows increased the momentum exchange between adjacent jets and heat dilution, enabling the WCJ system to lower net heat despite excessive solar and conductive heat gains. This nozzle configuration minimized localized hot spots and facilitated more uniform temperature distribution within the occupied zone. Higher n reduced the magnitude and duration of P_{net} peaks by up to 25%, accelerated post-peak decay, and produced flatter profiles with lower overall net heat. These results suggest that optimizing the number and arrangement of nozzles can significantly enhance cooling efficiency and thermal homogeneity in greenhouse environments.

A comparison of runs with unshaded and shaded external walls in summer reveals that shading reduces midday P_{net} peaks by approximately 15–30%, particularly during peak solar hours, when it limits solar absorption and heat inflow. This lowers the WCJ system's thermal load and P_{net} peaks, demonstrating that shading is a simple, cost-effective passive strategy to reduce daytime heat gains. However, because fixed shading can restrict nighttime cooling, adaptive or retractable designs are recommended to block midday radiation while enabling nocturnal heat release, thereby reducing daytime peaks, fan energy use, and crop heat stress, consistent with previous results that shading supports a favorable greenhouse microclimate [44].

The results of this study should be considered in light of several experimental and methodological limitations. The test room was intentionally left unoccupied to isolate thermal effects and crop-related interactions, such as aerodynamic resistance, crop-microclimate interactions, and heat exchange, which typically influence greenhouse thermal performance. Some environmental factors, including humidity, longwave radiation, and wind effects, were not directly measured, constraining the overall power balance assessment. In addition, the fixed airflow rate, due to the limited cooling capacity of the air-handling unit and the use of a single polycarbonate glazing material in one climatic context, limits the generalizability of the results. Despite these constraints, the study establishes a valuable baseline for evaluating the cooling performance of the WCJ system. This study underscores the need for future research that incorporates live plants, variable ventilation, and comprehensive environmental monitoring to enhance applicability across diverse greenhouse conditions.

4. Conclusions

This study experimentally evaluated the performance of a wall confluent jet (WCJ) cooling system in a greenhouse under real summer and autumn boundary conditions, examining the influence of the number of nozzle rows (n), room air temperature setpoint (T_{spt}), and external wall shading on cooling effectiveness, thermal uniformity, and energy performance. The results demonstrate that WCJ cooling can effectively mitigate solar heat gains, enhance convective heat transfer, and stabilize and control greenhouse indoor microclimates.

Increasing the T_{spt} reduced inlet air cooling by 25%, allowing warmer air to enter the indoor space and inadvertently decreasing the cooling load. Increasing T_{spt} by 4 °C raised the indoor air temperatures by 20–25%. Increasing the T_{spt} raised the ceiling, external wall, and floor surface temperatures by 17%, 20%, and 16%, respectively. Increasing the n lowered ceiling, wall, and floor surface temperatures by up to 8% and reduced indoor air temperature by about 6%.

External wall shading proved to be an effective passive measure for reducing solar and conductive heat gains. Shading lowered ceiling, external wall, and floor surface temperatures by 10%, 20–30%, and 10–20%, respectively, and reduced indoor peak air temperatures by up to 35% compared to unshaded summer conditions. The heat balance analysis indicated that shading suppressed net power peaks by up to 40%, enhanced cooling uniformity, and improved post-peak recovery, confirming that WCJ cooling can dynamically adapt to fluctuating solar loads.

Seasonal climatic comparisons confirmed that milder autumn conditions reduced net power loads by up to 50% compared with summer, indicating lower cooling requirements. Summer experiments revealed higher solar heat gain leading to higher cooling demand, with daytime indoor air temperatures exceeding those in autumn by 10–30%. Overall, the WCJ cooling system dynamically adjusted the inlet air temperature between 14 and 25 °C to track varying solar heat gains, thereby maintaining indoor air temperature within ±1.5 °C of the setpoint.

Future work should build on these results by conducting coupled experimental and numerical studies with live crops, accounting for radiative and latent heat exchanges and variable airflow rate, to develop predictive models and energy-optimized WCJ cooling controls. Future research coupling WCJ cooling systems with renewable or waste-heat-driven chillers offers a promising pathway toward sustainable, low-carbon, and climate-resilient greenhouse operations.

Author Contributions: Conceptualization, B.M. and G.C.; methodology, A.K., B.M. and G.C.; validation, B.M., A.K. and G.C.; formal analysis, G.C., A.K. and B.M.; investigation, G.C.; resources, B.M. and G.C.; writing—original draft preparation, G.C.; writing—review and editing, G.C., A.K. and B.M.; supervision, B.M. and A.K.; project administration, B.M. and G.C.; funding acquisition, B.M. All authors have read and agreed to the published version of the manuscript.

Funding: This work was funded by the Swedish Energy Agency [project ID number 52686-1].

Data Availability Statement: The raw data supporting the conclusions of this article will be made available by the authors upon request.

Acknowledgments: The authors acknowledge the support from the University of Gävle and the Swedish Energy Agency. They thank Patrick Olsson, Elisabet Linden, Rickard Larsson, and Mikael Sundberg for their technical help with data acquisition and Hofors municipality for providing the greenhouse for field studies.

Conflicts of Interest: The authors declare no conflicts of interest. The funders had no role in the design of the study; in the collection, analyses, or interpretation of data; in the writing of the manuscript; or in the decision to publish the results.

Abbreviations

The following abbreviations are used in this manuscript:

WCJ	Wall confluent jets
CJ	Confluent jets
AHU	Air handling unit
HVAC	Heating, ventilation, and air conditioning
CCAs	Constant Current Anemometers
n	Number of nozzle rows on the WCJ inlet diffuser [-]
T_{spt}	Room air Temperature setpoint [°C].
$\dot{V}$	Inlet airflow rate [m^3/s]
d	Internal diameter of nozzle [m]
P_{net}	Net power [W]
$P_{solar,transmitted}$	Transmitted solar power [W]
$P_{solar,absorbed}$	Floor absorbed solar power [W]
P_{cool}	WCJ convective cooling power [W]
P_{floor}	Floor re-radiated power [W]
P_{cond}	Conductive power [W]
I_{roof}	Solar radiation on the roof [W/m^2]
I_{ext_wall}	Solar radiation on the external wall [W/m^2]
A_{roof}	Roof area [m^2]
A_{ext_wall}	External wall area [m^2]
τ_{roof}	Solar transmittance through the roof [-]
τ_{ext_wall}	Solar transmittance through the external wall [-]
$F_{roof \rightarrow floor}$	View factor from the roof to the floor [-]
$F_{ext_wall \rightarrow floor}$	View factor from the external wall to the floor [-]
α_{floor}	Floor solar absorptance [-]
T_{floor}	Floor surface temperature [°C]
T_{in}	Inlet air temperature [°C]
T_{flm}	Film temperature of the air in the boundary layer along the floor [°C]
T_{indoor}	Indoor air temperature [°C]
U_{roof}	U-value of the honeycomb polycarbonate on the roof [$W/m^2.K$]
$U_{ext\,wall}$	U-value of the honeycomb polycarbonate on the external walls [$W/m^2.K$]
$U_{sidewall}$	U-value of the honeycomb polycarbonate on shaded sidewalls [$W/m^2.K$]
$T_{ceiling}$	Ceiling surface temperature [°C]
T_{roof}	Roof surface temperature [°C]
$T_{ext_wall_inner}$	Inner surface temperature of the external wall [°C]
$T_{ext_wall_outer}$	Outer surface temperature of the external wall [°C]
$T_{sidewall_inner}$	Inner surface temperature of the shaded sidewall [°C]
$T_{sidewall_outer}$	Outer surface temperature of the shaded sidewall [°C]
h	Convective heat transfer coefficient [$W/m^2.K$]
k	Thermal Conductivity [W/m·K]
Re_L	Reynolds number [-]
Pr	Prandtl number [-]

References

1. Ortega Alba, S.; Manana, M. Energy research in airports: A review. *Energies* **2016**, *9*, 349. [CrossRef]
2. Lu, Y.; Dong, J.; Liu, J. Zonal modelling for thermal and energy performance of large space buildings: A review. *Renew. Sustain. Energy Rev.* **2020**, *133*, 110241. [CrossRef]
3. Palmowska, A.; Miczka, G. Research on the thermal conditions in ventilated large space building. *ACEE J.* **2018**, *11*, 169–178. [CrossRef]
4. De Gelder, A.; Dieleman, J.A.; Bot, G.P.A.; Marcelis, L.F.M. An overview of climate and crop yield in closed greenhouses. *J. Hortic. Sci. Biotechnol.* **2012**, *87*, 193–202. [CrossRef]

5. Montero, J.I.; Teitel, M.; Baeza, E.; Lopez, J.C.; Kacira, M. Greenhouse design and covering materials. In *Good Agricultural Practices for Greenhouse Vegetable Crops*; FAO: Rome, Italy, 2013; p. 35.
6. Kim, H.-K.; Lee, S.-Y.; Kwon, J.-K.; Kim, Y.-H. Evaluating the effect of cover materials on greenhouse microclimates and thermal performance. *Agronomy* **2022**, *12*, 143. [CrossRef]
7. Reilly, A.; Kinnane, O. The impact of thermal mass on building energy consumption. *Appl. Energy* **2017**, *198*, 108–121. [CrossRef]
8. Jeon, J.; Lee, J.; Ham, Y. Quantifying the impact of building envelope condition on energy use. *Build. Res. Inf.* **2019**, *47*, 404–420. [CrossRef]
9. Kittas, C.; Baille, A.; Giaglaras, P. Influence of covering material and shading on the spectral distribution of light in greenhouses. *J. Agric. Eng. Res.* **1999**, *73*, 341–351. [CrossRef]
10. Samat, A.T.; Soltabayeva, A.; Bekturova, A.; Zhanassova, K.; Auganova, D.; Masalimov, Z.; Srivastava, S.; Satkanov, M.; Kurmanbayeva, A. Plant responses to heat stress and advances in mitigation strategies. *Front. Plant Sci.* **2025**, *16*, 1638213. [CrossRef] [PubMed]
11. Baille, A. Overview of greenhouse climate control in the mediterranean regions. *Cah. Options Méditerranéennes* **1999**, *31*, 59–76.
12. Sethi, V.P.; Sharma, S.K. Survey of cooling technologies for worldwide agricultural greenhouse applications. *Sol. Energy* **2007**, *81*, 1447–1459. [CrossRef]
13. Singh, M.C.; Singh, J.P.; Pandey, S.K.; Cutting, N.G.; Sharma, P.; Shrivastav, V.; Sharma, P. A review of three commonly used techniques of controlling greenhouse microclimate. *Int. J. Curr. Microbiol. App. Sci* **2018**, *7*, 3491–3505. [CrossRef]
14. Karimipanah, T.; Awbi, H.B. Theoretical and experimental investigation of impinging jet ventilation and comparison with wall displacement ventilation. *Build. Environ.* **2002**, *37*, 1329–1342. [CrossRef]
15. Awbi, H.B. *Ventilation of Buildings*; Routledge: Oxfordshire, UK, 2002; ISBN 1135817413.
16. Janbakhsh, S.; Moshfegh, B. Experimental investigation of a ventilation system based on wall confluent jets. *Build. Environ.* **2014**, *80*, 18–31. [CrossRef]
17. Andersson, H. *Optimization of Confluent Jets Ventilation with Variable Airflow*; Gävle University Press: Gävle, Sweden, 2022. Available online: https://www.diva-portal.org/smash/record.jsf?dswid=667&pid=diva2%3A1702356 (accessed on 26 October 2023).
18. Janbakhsh, S. *A Ventilation Strategy Based on Confluent Jets: An Experimental and Numerical Study*; Linköping University Electronic Press: Linköping, Sweden, 2015; Volume 1671. Available online: https://www.diva-portal.org/smash/get/diva2:808188/FULLTEXT02.pdf (accessed on 23 September 2021).
19. Svensson, K. *Experimental and Numerical Investigations of Confluent Round Jets*; Linköping University Electronic Press: Linköping, Sweden, 2015. Available online: https://www.diva-portal.org/smash/record.jsf?dswid=667&pid=diva2%3A805327 (accessed on 15 September 2020).
20. Janbakhsh, S.; Moshfegh, B.; Ghahremanian, S. A newly designed supply diffuser for industrial premises. *Int. J. Vent.* **2010**, *9*, 59–67. [CrossRef]
21. Svensson, K.; Rohdin, P.; Moshfegh, B. A computational parametric study on the development of confluent round jet arrays. *Eur. J. Mech.* **2015**, *53*, 129–147. [CrossRef]
22. Ghahremanian, S. *A Near-Field Study of Multiple Interacting Jets: Confluent Jets*; Linkopings Universitet: Linköping, Sweden, 2014. [CrossRef]
23. Choonya, G.; Kabanshi, A.; Moshfegh, B. Experimental Investigation of Wall Confluent Jets on Transparent Large-Space Building Envelopes: Part 1—Application in Heating Greenhouses. *Energies* **2024**, *17*, 6217. [CrossRef]
24. Peet, M.M.; Welles, G.W.H. Greenhouse tomato production. *Crop Prod. Sci. Hortic.* **2005**, *13*, 257–304. [CrossRef]
25. Willits, D.H.; Peet, M.M. The effect of night temperature on greenhouse grown tomato yields in warm climates. *Agric. For. Meteorol.* **1998**, *92*, 191–202. [CrossRef]
26. Bruun, H.H. Hot-wire anemometry: Principles and signal analysis. *Meas. Sci. Technol.* **1996**, *7*, 24. [CrossRef]
27. Lomas, C.G. *Fundamentals of Hot Wire Anemometry*; Cambridge University Press: Cambridge, UK, 2011; ISBN 0521283183.
28. Duff, M.; Towey, J. Two ways to measure temperature using thermocouples feature simplicity, accuracy, and flexibility. *Analog Dialogue* **2010**, *44*, 1–6.
29. Duffie, J.A.; Beckman, W.A.; Blair, N. *Solar Engineering of Thermal Processes, Photovoltaics and Wind*; John Wiley & Sons: Hoboken, NJ, USA, 2020; ISBN 1119540283.
30. Beaubien, D.J.; Bisberg, A.; Beaubien, A.F. Investigations in pyranometer design. *J. Atmos. Ocean. Technol.* **1998**, *15*, 677–686. [CrossRef]
31. Sager, R.; Petersen, N.H.; Wirsum, M. A Thermodynamic-Based Black-Box Modeling Approach for the Comprehensive Analysis of Vortex Tube Applications. *Energies* **2024**, *17*, 4180. [CrossRef]

32. Macrolux. Polycarbonate 16 mm Storm Panel the Ultimate Light Weight Translucent Storm Protection. Designed to Protect Your Windows and Doors from Hurricane and Severe Weather Winds, While at the Same Time Allowing Light in Macrolux® Polycarbonate Storm Panel i. Available online: https://www.macroluxusa.com/supports/01.-%20Macrolux%20Storm%20Panel%20USA-APR23-LOW.pdf? (accessed on 26 October 2025).
33. Zapałowicz, Z.; Wojnicki, O. Estimation of Total Solar Transmittance for Twin-Wall Polycarbonate Sheet with Rectangular Structure on the Basis of Experimental Research. *Energies* **2022**, *15*, 1360. [CrossRef]
34. Incropera, F.P.; DeWitt, D.P.; Bergman, T.L.; Lavine, A.S. *Fundamentals of Heat and Mass Transfer*; Wiley: New York, NY, USA, 1996; Volume 6.
35. Al-Helal, I.M.; Abdel-Ghany, A.M. Energy partition and conversion of solar and thermal radiation into sensible and latent heat in a greenhouse under arid conditions. *Energy Build.* **2011**, *43*, 1740–1747. [CrossRef]
36. Kadoya, K.; Matsunaga, N.; Nagashima, A. Viscosity and thermal conductivity of dry air in the gaseous phase. *J. Phys. Chem. Ref. Data* **1985**, *14*, 947–970. [CrossRef]
37. Holman, J.P. *Heat Transfer*, 10th ed.; McGraw-Hill Education: Blacklick, OH, USA, 2009; ISBN 978-0-07-352936-3.
38. Soussi, M.; Chaibi, M.T.; Buchholz, M.; Saghrouni, Z. Comprehensive review on climate control and cooling systems in greenhouses under hot and arid conditions. *Agronomy* **2022**, *12*, 626. [CrossRef]
39. Tsuchiya, R.; Okushima, L.; Ishii, M.; Moriyama, H. Effects of Concrete Block Flooring on Greenhouse Microclimate and Floor Surface Heat Balance. *Japan Agric. Res. Q. JARQ* **2023**, *57*, 37–45. [CrossRef]
40. Catrini, P.; Curto, D.; Franzitta, V.; Cardona, F. Improving energy efficiency of commercial buildings by Combined Heat Cooling and Power plants. *Sustain. Cities Soc.* **2020**, *60*, 102157. [CrossRef]
41. Ebrahimi, K.; Jones, G.F.; Fleischer, A.S. A review of data center cooling technology, operating conditions and the corresponding low-grade waste heat recovery opportunities. *Renew. Sustain. Energy Rev.* **2014**, *31*, 622–638. [CrossRef]
42. Liu, W.H.; Hashim, H.; Lim, J.S.; Ho, C.S.; Klemeš, J.J.; Zamhuri, M.I.; Ho, W.S. Techno-economic assessment of different cooling systems for office buildings in tropical large city considering on-site biogas utilization. *J. Clean. Prod.* **2018**, *184*, 774–787. [CrossRef]
43. Santolini, E.; Pulvirenti, B.; Guidorzi, P.; Bovo, M.; Torreggiani, D.; Tassinari, P. Analysis of the effects of shading screens on the microclimate of greenhouses and glass facade buildings. *Build. Environ.* **2022**, *211*, 108691. [CrossRef]
44. Ahemd, H.A.; Al-Faraj, A.A.; Abdel-Ghany, A.M. Shading greenhouses to improve the microclimate, energy and water saving in hot regions: A review. *Sci. Hortic.* **2016**, *201*, 36–45. [CrossRef]

Disclaimer/Publisher's Note: The statements, opinions and data contained in all publications are solely those of the individual author(s) and contributor(s) and not of MDPI and/or the editor(s). MDPI and/or the editor(s) disclaim responsibility for any injury to people or property resulting from any ideas, methods, instructions or products referred to in the content.